Magnetic moments of the $\Lambda(1405)$ and $\Lambda(1670)$ resonances

D. Jido[1], A. Hosaka[2], J.C. Nacher[3], E. Oset[3] and A. Ramos[1]

[1] *Departament d'Estructura i Constituents de la Matèria,*
Universitat de Barcelona, Diagonal 647, 08028 Barcelona, Spain
[2] *Research Center for Nuclear Physics (RCNP), Osaka University,*
Ibaraki, Osaka 567-0047, Japan
[3] *Departamento de Física Teórica and IFIC,*
Centro Mixto Universidad de Valencia-CSIC,
Ap. Correos 22085, E-46071 Valencia, Spain

Abstract

By using techniques of unitarized chiral perturbation theory, where the $\Lambda(1405)$ and $\Lambda(1670)$ resonances are dynamically generated, we evaluate the magnetic moments of these resonances and their transition magnetic moment. The results obtained here differ appreciably from those obtained with existing quark models. The width for the $\Lambda(1670) \to \Lambda(1405)\gamma$ transition is also evaluated leading to a branching ratio of the order of 2×10^{-6}.

1 Introduction

The evaluation of static properties of baryonic resonances, like the magnetic moment, is a standard exercise when one has a wave function for the states. This is the case of the quark models where a thorough investigation of magnetic moments and other static properties [1], such as masses and couplings to the πN system [2], has been done.

The introduction of unitary chiral techniques has allowed one to show that the octet of the lowest energy $J^P = 1/2^-$ baryonic resonances can be generated dynamically from the lowest order chiral Lagrangian and by the use of natural size cut-offs or regularizing scales to make the divergent loop integrals finite. These findings allow one to classify those states as quasibound meson-baryon states, or equivalently, ordinary multiple scattering resonances in coupled channels. The $\Lambda(1405)$ was one of the first resonances to receive attention from the chiral unitary perspective [3, 4, 5]. The $N^*(1535)$ was also

generated within chiral unitary schemes in [6, 7, 8] and has been recently revised in [9] with the inclusion of $\pi\pi N$ channels. Recently the $\Lambda(1670)$ and $\Sigma(1620)$ [10] and the $\Xi(1620)$ states [11] have also been generated within the same scheme, thus completing the octet of dynamically generated states.

In the chiral unitary method, one computes scattering matrices in all meson and baryon channels and poles for resonances are searched in the second Riemann sheet. The poles provide the mass and the width of the resonance states and, in addition, the residues at the poles provide the product of the couplings of the resonance to the initial and final states of the considered transition scattering matrix element. In this method, it is not straightforward to evaluate other properties of the resonance, like magnetic moments, since, unlike ordinary quantum mechanical problems, in the present approach we do not have wave functions and operators manifestly. Therefore, we need to explore an alternative method to compute resonance magnetic moments from scattering matrices. This is the subject of the present work. We compute the magnetic moments of the $\Lambda(1405)$ and $\Lambda(1670)$ resonances, as well as the transition magnetic moment from the $\Lambda(1670)$ to the $\Lambda(1405)$, which allows us to determine the partial decay width for the decay $\Lambda(1670) \rightarrow \Lambda(1405)\gamma$. We also compare the results obtained here with those of ordinary quark models showing that there are appreciable differences between them. This offers an evidence that the nature of these states as dynamically generated from multiple scattering of coupled channels of mesons and baryons differs from an ordinary quark model description.

The paper is organized as follows. In section 2, we briefly describe the model that we use and show in detail the method to compute scattering matrices. In section 3, we compare the scattering matrices with a resonance dominant form and extract the magnetic moments. In section 4, we present our numerical results, which are compared with quark model results in section 5. The final section summarizes our findings.

2   Evaluation of the magnetic moment

The procedure to evaluate the magnetic moment of the resonances proceeds in an analogous way to that for the $N^*N^*\pi$ coupling in [7]. We evaluate the T-matrix for the process $MB \rightarrow M'B'\gamma$ using the chiral Lagrangian for the coupling of the mesons and baryons and for the photon to the mesons and baryons. We sum the Feynman diagrams which generate the resonance both on the left and on the right of the photon coupling. Isolation of resonance poles from these diagrams then allows us to evaluate the resonance magnetic moment.

The $\Lambda(1405)$ resonance is generated in [4] by means of the Bethe-Salpeter equation with a cut-off to regularize the loop integrals. The Bethe-Salpeter

equation is given by

$$T = V + VGT \; , \tag{1}$$

where in the present method the term VGT is given as a matrix product of the potential V, the meson-baryon propagator G and the T-matrix T. The diagonal matrix G contains the loop integral of a meson and baryon propagators. In general, the product VGT involves an integral over off-shell momenta. In the present approach that integral is greatly simplified reducing the problem to a matrix product due to the on-shell factorizations of V and T. The on-shell factorization in [4] was done by incorporating the off-shell part of the loops into renormalization of couplings of the lowest order Lagrangian, in analogy to what was done in the meson-meson interaction in [12]. An explicit demonstration of the cancellation of these terms with tadpole corrections can also be seen in [13] for the p-wave meson-meson interaction in the ρ channel. The on-shell factorization allows one to solve eq.(1) to give

$$T = [1 - VG]^{-1} V \; , \tag{2}$$

in a simple matrix inversion. This has also been derived using the unitarization with the N/D method and dispersion relations in [5]. In this latter paper [5] the regularization of the loops is done by means of dimensional regularization with subtraction constants in the G function. The same method was used in [10] to obtain the $\Lambda(1405)$ and $\Lambda(1670)$ resonances, which is the one we follow here. The Feynman diagrams summed by eqs. (1) and (2) are given in Fig.1.

The s-wave meson-baryon interaction potential V is derived from the second order terms in the meson field of the chiral Lagrangian [14, 15]:

$$V_{ij} = -C_{ij} \frac{1}{4f^2} (2\sqrt{s} - M_i - M_j) \left(\frac{M_i + E}{2M_i} \right)^{1/2} \left(\frac{M_j + E'}{2M_j} \right)^{1/2} \; , \tag{3}$$

where the coefficients $C_{ij} (= C_{ji})$ are given in [4] and the meson decay constant f is taken as an average value $f = 1.123 f_\pi$. The G function for each meson-baryon channel is given by

$$
\begin{aligned}
G_l(\sqrt{s}) &= i 2 M_l \int \frac{d^4 q}{(2\pi)^4} \frac{1}{(P-q)^2 - M_l^2 + i\epsilon} \frac{1}{q^2 - m_l^2 + i\epsilon} \\
&= \frac{2M_l}{16\pi^2} \left\{ a(\mu) + \ln \frac{M_l^2}{\mu^2} + \frac{m_l^2 - M_l^2 + s}{2s} \ln \frac{m_l^2}{M_l^2} \right. \\
&\quad + \frac{\bar{q}_l}{\sqrt{s}} \left[\ln(s - (M_l^2 - m_l^2) + 2\bar{q}_l\sqrt{s}) + \ln(s + (M_l^2 - m_l^2) + 2\bar{q}_l\sqrt{s}) \right. \\
&\quad \left. \left. - \ln(-s + (M_l^2 - m_l^2) + 2\bar{q}_l\sqrt{s}) - \ln(-s - (M_l^2 - m_l^2) + 2\bar{q}_l\sqrt{s}) \right] \right\} \; ,
\end{aligned}
\tag{4}
$$

where m and M are taken to be the observed meson and baryon masses, respectively, and μ is a regularization scale which is chosen to be 630 MeV

3

as in [10]. The subtraction constants a_l are of the order of -2, which is a natural size as shown in [5]. The values chosen in [10], which reproduce the results of [4] calculated with just one cut-off, are

$$
\begin{aligned}
a_{\bar{K}N} &= -1.84, \quad a_{\pi\Sigma} = -2.00, \quad a_{\pi\Lambda} = -1.83 \\
a_{\eta\Lambda} &= -2.25, \quad a_{\eta\Sigma} = -2.38, \quad a_{K\Xi} = -2.67
\end{aligned}
\tag{5}
$$

The elementary couplings of the photon to the components of the meson-baryon amplitude at lowest order of the chiral expansion are shown in fig.2. Now if we want to generate the resonance on the left and right sides of the photon coupling we must consider the diagrams shown in fig.3. The diagrams of row b) in fig.3 vanish, given the s-wave nature of the meson-baryon vertices and the $\vec{\epsilon} \cdot \vec{q}_L$ coupling of the photon to the mesons, which makes the integral over the loop variable q_L vanish. The remaining couplings are those of the photon to the baryons and the analogous ones with two extra meson lines. The spin dependent part of these couplings needed for the evaluation of magnetic moments is given by [16]

$$
\mathcal{L} = -\frac{i}{4M_p} b_6^F \langle \bar{B}[S^\mu, S^\nu][F_{\mu\nu}^+, B] \rangle - \frac{i}{4M_p} b_6^D \langle \bar{B}[S^\mu, S^\nu]\{F_{\mu\nu}^+, B\} \rangle
\tag{6}
$$

with

$$
\begin{aligned}
F_{\mu\nu}^+ &= -e(u^\dagger Q F_{\mu\nu} u + u Q F_{\mu\nu} u^\dagger) \\
F_{\mu\nu} &= \partial_\mu A_\nu - \partial_\nu A_\mu ,
\end{aligned}
\tag{7}
\tag{8}
$$

where M_p is the mass of proton, A_μ is the electromagnetic field, and b_6^F and b_6^D are parameters to be fitted so as to reproduce the magnetic moments of the ground state baryons. In eq.(6), $\langle \cdots \rangle$ means the trace over flavor indices, B is the SU(3) matrix for the baryon field [14, 15], and S^μ are spin matrices as explained below. In eq.(7) Q is the charge matrix for the u, d, s quarks: $Q = \frac{1}{3}\text{diag}(2, -1, -1)$ and $u^2 = U = \exp(i\sqrt{2}\Phi/f)$ where Φ is the SU(3) matrix of the pseudoscalar meson field [14, 15, 17]. In the baryon rest frame the operator S^μ becomes $\vec{\sigma}/2$ and then,

$$
[S^\mu, S^\nu]F_{\mu\nu} \to -(\vec{\sigma} \times \vec{q}) \cdot \vec{\epsilon}
\tag{9}
$$

in the Coulomb gauge ($\epsilon^0 = 0$, $\vec{\epsilon} \cdot \vec{q} = 0$) and for an outgoing photon. Thus the vertex from the Lagrangian of eq.(6) can be written as

$$
\mathcal{L} \to e\frac{\vec{\sigma} \times \vec{q}}{2M_p} \cdot \vec{\epsilon} \left(-\frac{i}{2} b_6^F \left\langle \bar{B}[(u^\dagger Q u + u Q u^\dagger), B] \right\rangle \right.
\tag{10}
$$

$$
\left. -\frac{i}{2} b_6^D \left\langle \bar{B}\{(u^\dagger Q u + u Q u^\dagger), B\} \right\rangle \right) .
\tag{11}
$$

4

	p	n	Σ^+	Σ^-	Σ^0	Λ	$(\Lambda\Sigma^0)$	Ξ^-	Ξ^0
d_i	$\frac{1}{3}$	$-\frac{2}{3}$	$\frac{1}{3}$	$\frac{1}{3}$	$\frac{1}{3}$	$-\frac{1}{3}$	$\frac{1}{\sqrt{3}}$	$\frac{1}{3}$	$-\frac{2}{3}$
f_i	1	0	1	-1	0	0	0	-1	0

Table 1: d_i and f_i coefficient of eq.(12).

	K^-p	$\bar{K}^0n$	$\pi^0\Lambda$	$\pi^0\Sigma^0$	$\eta\Lambda$	$\eta\Sigma^0$	$\pi^+\Sigma^-$	$\pi^-\Sigma^+$	$K^+\Xi^-$	$K^0\Xi^0$
K^-p	0	$-\frac{1}{2}$	$-\frac{1}{4\sqrt{3}}$	$\frac{1}{4}$	$-\frac{1}{4}$	$\frac{3}{4\sqrt{3}}$	0	1	0	0
$\bar{K}^0n$		0	0	0	0	0	$-\frac{1}{2}$	0	0	0
$\pi^0\Lambda$			0	0	0	0	$\frac{1}{\sqrt{3}}$	$\frac{1}{\sqrt{3}}$	$-\frac{1}{4\sqrt{3}}$	0
$\pi^0\Sigma^0$				0	0	0	0	0	$\frac{1}{4}$	0
$\eta\Lambda$					0	0	0	0	$-\frac{1}{4}$	0
$\eta\Sigma^0$						0	0	0	$\frac{3}{4\sqrt{3}}$	0
$\pi^+\Sigma^-$							0	0	1	0
$\pi^-\Sigma^+$								0	0	$-\frac{1}{2}$
$K^+\Xi^-$									0	$-\frac{1}{2}$
$K^0\Xi^0$										0

Table 2: X_{ij} coefficient of eq.(14). $X_{ij} = X_{ji}$

By expanding u in terms of the meson field we obtain the expressions for both the $\gamma BB'$ and $\gamma BB'MM'$ vertices. By taking $u = 1$ we obtain the magnetic moments of the ground state octet baryons,

$$\mu_i = d_i b_6^D + f_i b_6^F \; , \tag{12}$$

where the coefficients d_i and f_i are given in table 1. One immediately realizes that by setting $b_6^D = 0$ and $b_6^F = 1$ one obtains the ordinary magnetic moments of the baryons without anomalous contributions. Fitting the values of eq.(12) to the observed magnetic moments of the baryons one obtains

$$b_6^D = 2.40, \qquad b_6^F = 1.82 \tag{13}$$

very similar to those given in [16], $b_6^D = 2.39, b_6^F = 1.77$.

Similarly, by expanding u up to two meson fields we obtain the vertices of diagram a) of fig.2 with the result

$$- it_{ij}^{a)} = \frac{e}{2M_p}(\vec{\sigma} \times \vec{q}) \cdot \vec{\epsilon}\frac{1}{2f^2}[X_{ij}b_6^D + Y_{ij}b_6^F] \; , \tag{14}$$

where the coefficients X_{ij} and Y_{ij} are given in tables 2 and 3.

The evaluation of the amplitudes corresponding to the diagrams of fig.3 (the magnetic part) is straightforward. We obtain,

$$- it_{ij}^{\gamma} = -i\tilde{t}_{ij}\frac{e}{2M_p}(\vec{\sigma} \times \vec{q}) \cdot \vec{\epsilon} \tag{15}$$

	K^-p	$\bar{K}^0n$	$\pi^0\Lambda$	$\pi^0\Sigma^0$	$\eta\Lambda$	$\eta\Sigma^0$	$\pi^+\Sigma^-$	$\pi^-\Sigma^+$	$K^+\Xi^-$	$K^0\Xi^0$
K^-p	-2	$-\frac{1}{2}$	$-\frac{3}{4\sqrt{3}}$	$-\frac{1}{4}$	$-\frac{3}{4}$	$-\frac{3}{4\sqrt{3}}$	0	-1	0	0
$\bar{K}^0n$		0	0	0	0	0	$\frac{1}{2}$	0	0	0
$\pi^0\Lambda$			0	0	0	0	0	0	$\frac{3}{4\sqrt{3}}$	0
$\pi^0\Sigma^0$				0	0	0	1	-1	$\frac{1}{4}$	0
$\eta\Lambda$					0	0	0	0	$\frac{3}{4}$	0
$\eta\Sigma^0$						0	0	0	$\frac{3}{4\sqrt{3}}$	0
$\pi^+\Sigma^-$							2	0	1	0
$\pi^-\Sigma^+$								-2	0	$-\frac{1}{2}$
$K^+\Xi^-$									2	$\frac{1}{2}$
$K^0\Xi^0$										0

Table 3: Y_{ij} coefficient of eq.(14). $Y_{ij} = Y_{ji}$

and

$$- i\tilde{t}_{ij} = \left(\sum_{lm} t_{il}G_l A_{lm}G_m t_{mj} + \sum_{l} t_{il}\tilde{G}_l t_{lj}\mu_{B_l} \right) . \qquad (16)$$

In this equation t_{ij} is the scattering amplitude from the channel i to j,

$$A_{lm} = \frac{1}{2f^2}[X_{lm}b_6^D + Y_{lm}b_6^F] , \qquad (17)$$

and

$$\tilde{G}_l(p) = i \int \frac{d^4k}{(2\pi)^4} D(k)G(p-k)G(p-k) \qquad (18)$$

with D and G the meson and baryon propagators. Here, by keeping up to linear terms in q, we have neglected the small momentum of the photon in the second baryon propagator. Therefore, we can write

$$\tilde{G}_l(\sqrt{s}) = -\frac{\partial}{\partial\sqrt{s}}G_l . \qquad (19)$$

This approximation allows us to obtain an analytic expression for $\tilde{G}_l(\sqrt{s})$. In eq.(16), we omit to write contributions from the Λ-Σ^0 transition magnetic moment. The contributions are negligible since the Λ-Σ^0 transition changes the isospin, therefore either the left or right resonances must have isospin 1, which is not the present case.

3 Comparison to the resonance description

In order to extract a resonance magnetic moment from the scattering amplitude, (15) or (16), we assume that resonances are dynamically generated

on the left and right of the photon coupling. First we parameterize the meson-baryon scattering amplitude t_{ij} as shown in fig.4(b) by the resonance dominant Breit-Wigner form:

$$-it_{ij} = -ig_i \frac{i}{\sqrt{s} - M_R + i\Gamma/2} (-ig_j^*) . \tag{20}$$

Here we have introduced the resonance mass M_R, the total decay width Γ and the decay constant to the channel i, g_i. Then the photon coupling amplitude t_{ij}^γ is parameterized as shown in fig.4(a) by the expression:

$$-it_{ij}^\gamma = -ig_i \frac{i}{\sqrt{s} - M_R + i\Gamma/2} \frac{e\mu_{\Lambda^*}}{2M_p} (\vec{\sigma} \times \vec{q}) \cdot \vec{\epsilon} \frac{i}{\sqrt{s} - M_R + i\Gamma/2} (-i)g_j^* . \tag{21}$$

Dividing $-it_{ij}^\gamma$ by t_{ij} and by $\frac{e}{2M_p}(\vec{\sigma} \times \vec{q}) \cdot \vec{\epsilon}$ we cancel the coupling constants and one propagator. Thus by evaluating this ratio at the Λ^* pole, where the amplitudes are dominated by the resonance, and recalling eq.(15), we have

$$\mu_{\Lambda^*} = \lim_{z \to z_R} (z - z_R) \frac{-i\tilde{t}_{ij}(z)}{t_{ij}(z)} = \text{Res} \frac{-i\tilde{t}_{ij}(z)}{t_{ij}(z)} \bigg|_{z=z_R} . \tag{22}$$

where z_R denotes the position of the pole in the second Riemann sheet, $z_R \equiv M_R + i\Gamma/2$. In fact, there exist two poles around the region of the $\Lambda(1405)$ [5], located at $z_R = 1426 + 16i$ and $1390 + 66i$ MeV. The former pole largely couples to the $\bar{K}N$ state, whereas the latter one couples predominantly to the $\pi\Sigma$ state. Both poles may contribute to the resonance $\Lambda(1405)$. We evaluate the magnetic moment at both poles. For the $\Lambda(1670)$ the pole position is $z_R = 1680 + 20i$ MeV.

Similarly, we can also evaluate the transition amplitude between the $\Lambda(1670)$ and $\Lambda(1405)$ resonances. This is accomplished by putting different energies, $\sqrt{s_1}$ and $\sqrt{s_2}$, on the transition amplitudes t_{ij} appearing on the left and right of the photon coupling in eq. (16). Then by taking $\sqrt{s_1} \equiv z_{1R}$ for the first resonance ($\Lambda(1670)$) and $\sqrt{s_2} \equiv z_{2R}$ for the second resonance ($\Lambda(1405)$), we would find

$$\mu_{\Lambda(1670) \to \Lambda(1405)} = \lim_{\substack{z_1 \to z_{1R} \\ z_2 \to z_{2R}}} \frac{-i\tilde{t}_{ij}(z_1, z_2)g_i(1670)g_j^*(1405)}{t_{ii}(z_1)t_{jj}(z_2)} . \tag{23}$$

The analysis in the complex plane has the advantage of making the background contributions negligible since the evaluations are done exactly at the poles of the resonances. The magnetic moment evaluated in the complex plane, however, has a complex value, which might induce uncertainties since one is extrapolating from the real axis to the complex plane. Hence, to avoid these uncertainties, we also calculate the amplitudes on the real axis in the first Riemann sheet. The magnetic moments are then defined by

$$\mu_{\Lambda^*} = \frac{-i\tilde{t}_{ij}(\sqrt{s})}{-\frac{\partial}{\partial\sqrt{s}}t_{ij}(\sqrt{s})} , \tag{24}$$

7

where both the coupling constants and the resonance propagators cancel to provide the magnetic moment of the resonance. In order to eliminate background we choose external channels which have a large coupling to the resonances and, furthermore, we take the $I = 0$ isospin combination. In particular, we take the $\bar{K}N$ state with $I = 0$ for $\Lambda(1405)$ and the $K\Xi$ state with $I = 0$ for $\Lambda(1670)$ because of their large couplings to the corresponding channels [10]. For $\Lambda(1405)$ we also calculate the magnetic moment in the $\bar{K}N \to \gamma\pi\Sigma$ channel, since this channel may be used in the experiments to determine the magnetic moment of the $\Lambda(1405)$. We show the numerator and the denominator of eq.(24) in fig.5 with the $\bar{K}N$ channel, in fig.6 with the $\bar{K}N \to \gamma\pi\Sigma$ for the $\Lambda(1405)$ and in fig.7 with the $K\Xi$ channel for the $\Lambda(1670)$. We take the ratio of these amplitudes around the energy close to the resonance where the real part of the two functions has maximum strength. In order to estimate uncertainties we also evaluate the ratio at the point where either the imaginary part of the numerator or denominator becomes zero, as well as the ratio of the dominant real parts. In principle, in the absence of background contamination, these evaluations should give the same value.

As for the transition magnetic moment, in order to cancel the couplings and propagators, we take the ratio

$$\mu^2_{\Lambda(1670)\to\Lambda(1405)} = \frac{(-i\tilde{t}_{K\Xi\to\gamma\bar{K}N}(\sqrt{s_1}, \sqrt{s_2}))(i\tilde{t}_{\bar{K}N\to\gamma K\Xi}(\sqrt{s_2}, \sqrt{s_1}))}{\left(-\frac{\partial}{\partial\sqrt{s}}t_{K\Xi}(\sqrt{s_1})\right)\left(-\frac{\partial}{\partial\sqrt{s}}t_{\bar{K}N}(\sqrt{s_2})\right)} \tag{25}$$

and we proceed as before to evaluate the ratio and the uncertainties. We show in fig.8 the numerator and the denominator of eq.(25), for fixed $\sqrt{s_2} = 1681$ MeV as a function of $\sqrt{s_1}$ in the left panels, and for fixed $\sqrt{s_1} = 1423$ MeV as a function of $\sqrt{s_2}$ in the right panels.

Experimentally, magnetic moments of resonances may be extracted from bremsstrahlung processes, which are carefully compared with theoretical models. On the other hand, the transition magnetic moment between $\Lambda(1670)$ and $\Lambda(1405)$ could be directly investigated from the decay $\Lambda(1670) \to \Lambda(1405)\gamma$. The width for this transition is given by

$$\Gamma = \frac{1}{\pi}\frac{M_{\Lambda(1405)}}{M_{\Lambda(1670)}}q^3\left(\frac{e\mu_{\Lambda(1670)\to\Lambda(1405)}}{2M_p}\right)^2 \tag{26}$$

with q the photon momentum in the $\Lambda(1670)$ rest frame.

4   Results

Comparison of the numerator and denominator in eq.(24) for the $\Lambda(1405)$ with the $\bar{K}N \to \gamma\bar{K}N$ and $\bar{K}N \to \gamma\pi\Sigma$ channel and performing the ratios discussed in the former section we obtain a value

$$\mu_{\Lambda(1405)} = +0.24 \sim 0.45 \tag{27}$$

8

	$\Lambda(1405)$	$\Lambda(1650)$	transition
real axis	$+0.44 \pm 0.06^{a)}$	-0.29 ± 0.01	0.023 ± 0.009
	$+0.26 \pm 0.07^{b)}$		
complex plane	$0.41 \pm 0.01^{c)}$	0.23	$0.019 \pm 0.002^{c)}$
(absolute value)	$0.30 \pm 0.01^{d)}$		$0.093 \pm 0.003^{d)}$

Table 4: Magnetic moments obtained by the chiral unitary approach in units of the nuclear magneton. The values without signs denote the modules. a) calculation in the $\bar{K}N \to \gamma \bar{K}N$ channel. b) calculation in the $\bar{K}N \to \gamma \pi \Sigma$ channel. c) taking $z_R = 1426 + 16i$ for $\Lambda(1405)$. d) taking $z_R = 1390 + 66i$ for $\Lambda(1405)$.

in units of the nuclear magneton $\mu_N = e/2M_p$. The large uncertainty in the result obtained comes from the energy range where the amplitudes of the ratio of eq.(24) are evaluated. As seen in figs. 5 and 6 the value of this energy, which signals the position of the resonance in the real axis, is around 1418-1422 MeV for the $\bar{K}N$ channel and 1403-1416 MeV for the $\pi \Sigma$ channel. The evaluation in the $\bar{K}N$ channel gives $\mu_{\Lambda(1405)} = +0.44 \pm 0.06$, while in the $\bar{K}N \to \gamma \pi \Sigma$ we obtain $+0.26 \pm 0.07$. We also evaluate the magnetic moment using the ratio of eq.(22) at the pole in the second Riemann sheet, which gives a complex number with the module 0.41 ± 0.01 for the case of $z_R = 1426 + 16i$ and 0.30 ± 0.01 for $z_R = 1390 + 66i$. All possible isospin $I = 0$ combinations, $\bar{K}N$, $\pi \Sigma$, $\eta \Lambda$ and $K\Xi$, provide approximately the same value (the channel dependence is shown in the small error bar of the presented value.) This channel insensitivity in the evaluation in the complex plane implies that the ratio of eq.(22) at the pole is dominated by the resonance and is not affected by background contaminations. It is interesting to note that the values in the complex plane are comparable with the value of eq.(27). In addition, recalling that the pole at $z_R = 1426 + 16i$ couples largely to $\bar{K}N$ and that at $z_R = 1390 + 66i$ to $\pi \Sigma$, the channel (or energy) dependence of the magnetic moment evaluated on the real axis stems from a different contribution of each pole to the values of the amplitudes in the real axis.

For the case of the $\Lambda(1670)$ the ratio obtained from fig.7 with the $K\Xi$ channel gives us

$$\mu_{\Lambda(1670)} = -0.29 \pm 0.01 \qquad (28)$$

with small uncertainty, and we find that the ratio of eq. (24) is stable around the resonance region. It is also interesting to note that the analysis in the complex plane in the pole in the second Riemann sheet (eq.(22)) gives in this case a value for the modulus of 0.23, which is similar to that of eq.(28). As in the preceding case, the analysis in the real plane allows us to obtain a real magnetic moment with a given sign.

Finally for the case of the transition magnetic moment we obtain the

value from eq.(25) and fig.8

$$\left|\mu_{\Lambda(1670)\to\Lambda(1405)}\right| = 0.023 \pm 0.009 \tag{29}$$

We also evaluate the transition magnetic moment from eq.(23) in the complex plane, which gives the modulus 0.019 ± 0.002 with $z_{1R} = 1680 + 20i$, $z_{2R} = 1426 + 16i$ and 0.093 ± 0.003 with $z_{1R} = 1680 + 20i$, $z_{2R} = 1390 + 66i$. The values obtained in the complex plane are less reliable in this case because they involve an extrapolation of two variables to the complex plane, each of which induces uncertainties. Even then, the agreement with the evaluation on the real axis is fair if we take into account the fact that, given the smallness of these numbers, their differences are of the same order of magnitude than those for the $\Lambda(1405)$ case. The results discussed here are summarized in table 4.

With the value of the transition magnetic moment of eq.(29) and using eq.(26) we obtain a partial width for the $\Lambda(1670) \to \Lambda(1405)\gamma$ decay which corresponds to a branching ratio 2×10^{-6}.

5 Quark Model Results

In this section we compute the resonance magnetic moments in the non-relativistic quark model. This demonstrates that the nature of the resonances differ appreciably from the chiral unitary description. In the $SU(6)$ quark model, the $\Lambda(1405)$ and $\Lambda(1670)$ are described as p-wave excitations of the 70-dimensional representation, whose $SU(2) \times SU(3)$ decomposition is given by

$$70 = {}^2 8 + {}^4 8 + {}^2 1 + {}^2 10 . \tag{30}$$

Here in the notation on the right hand side, ${}^{2j+1}D$, j represents the resonance spin and D the dimension of the flavor $SU(3)$ representation.

Since the Λ particles are isosinglet, their wave functions are spanned by the flavor octet and singlet states. Explicitly, these states are given as [20]

$$\begin{aligned}
|{}^2 8; jm\rangle &= \frac{1}{2} \left([\psi(\rho), \chi_\rho]_{jm}\phi_\lambda + [\psi(\rho), \chi_\lambda]_{jm}\phi_\rho \right. \\
&\quad \left. + [\psi(\lambda), \chi_\rho]_{jm}\phi_\rho + [\psi(\lambda), \chi_\lambda]_{jm}\phi_\lambda \right) , \\
|{}^4 8; jm\rangle &= \frac{1}{\sqrt{2}} \left([\psi(\lambda), \chi_S]_{jm}\phi_\lambda + [\psi(\rho), \chi_S]_{jm}\phi_\rho \right) , \\
|{}^2 1; jm\rangle &= \frac{1}{\sqrt{2}} \left([\psi(\lambda), \chi_\rho]_{jm} - [\psi(\rho), \chi_\lambda]_{jm} \right) \phi_A .
\end{aligned} \tag{31}$$

Here we have employed standard notations:

$$\vec{\rho} = \frac{1}{\sqrt{2}} (\vec{x}_2 - \vec{x}_1)$$

$$\vec{\lambda} = \frac{1}{\sqrt{6}} (\vec{x}_2 + \vec{x}_1 - 2\vec{x}_3)$$

$\psi(\vec{x}):$ p wave orbital wave functions

$\chi_{\rho,\lambda,S}:$ flavor wave functions of ρ, λ and S symmetry

$\phi_{\rho,\lambda,A}:$ flavor wave functions of ρ, λ and A symmetry

Furthermore, in eq. (31), the orbital and spin wave functions are coupled to the total spin jm.

In the non-relativistic description, the magnetic moment operator is given by the sum of twice the spin and the orbital angular momentum:

$$\vec{\mu} = \frac{e}{2m} \sum_{i=1}^{3} \left(\vec{\sigma}(i) + \vec{l}(i) \right) \left(\frac{1}{2}\lambda_3(i) + \frac{1}{2\sqrt{3}}\lambda_8(i) \right) . \tag{32}$$

In this equation m is a constituent quark mass for which we take for simplicity a common value $m \sim M_N/3$ for the three quarks. Furthermore, we have written the charge matrix as a sum of $SU(3)$ components. Due to the isosinglet nature of the Λ particles, the matrix elements of the isovector (λ_3) term vanish and only the λ_8-term contributes. The actual computation is straightforward and therefore here we present only the final result. By writing a Λ state as

$$|\Lambda\rangle = a_1|^28\rangle + a_2|^48\rangle + a_3|^21\rangle , \tag{33}$$

where the coefficients must satisfy the normalization condition, $a_1^2 + a_2^2 + a_3^3 = 1$, we find for the diagonal element:

$$\langle\Lambda|\mu_z|\Lambda\rangle = -\frac{1}{12}a_2^2 + \frac{1}{9}a_1 a_3 . \tag{34}$$

Similarly we can compute the off-diagonal matrix element.

The coefficients are determined by assuming suitable interactions between quarks. Here we employ two parameter sets; Isgur-Karl (IK) [1] and Hey-Litchfield-Cashmore (HLC) [19], the values of which are shown in Table 5. We summarize the results for the magnetic moments in Table 6, where the results for the transition magnetic moment are also shown. We find that the magnetic moment of the $\Lambda(1405)$ is small and negative, as opposed to the result of the chiral unitary method. For the $\Lambda(1670)$ the HLC parameters provide a value similar to the chiral unitary method. For the transition magnetic moment, however, the quark model values are significantly larger than the chiral unitary ones, by about a factor ten. This in turn results in the branching ratio in the $\Lambda(1670)$ decay about hundred times larger than the chiral unitary result. In general, the magnetic moments are sensitive to the choice of the mixing coefficients. However, absolute values are small for a reasonable range of the mixing parameters. In the quark model, there are two reasons for this:

	Λ(1405)			Λ(1670)		
	a_1	a_2	a_3	a_1	a_2	a_3
IK	0.43	0.06	0.9	0.75	0.58	−0.39
HLC	0.46	0.25	0.85	−0.04	−0.95	0.30

Table 5: Expansion coefficients in (33).

	Λ(1405)	Λ(1670)	|Λ(1405)-Λ(1670)|
IK	−0.13	0.01	0.14
HLC	−0.15	−0.23	0.26

Table 6: Magnetic moments in the quark model in units of nuclear magneton $e/2m_p$.

1. Only the isoscalar (λ_8) component contributes, which has relatively small contributions.

2. For spin doublet $^2 8$ and $^2 1$ states, the spin $\vec{s}$ and orbital angular momentum $\vec{l}$ are aligned such that their contributions roughly cancel. Classically, to form a $(jm) = (1/2, 1/2)$ state, $\vec{l}$ orients to the $+z$ direction, while $\vec{s}$ orients to the $-z$ directions; $\langle l_z \rangle = 1$ and $\langle s_z \rangle = -1/2$. The magnetic moment of this configuration vanishes:

$$\langle \mu_z \rangle = 1 \langle l_z \rangle + 2 \langle s_z \rangle = 0 \,. \tag{35}$$

6   Conclusion

We have introduced here the formalism to evaluate magnetic moments and the transition magnetic moment of the two Λ^* resonances, $\Lambda(1405)$ and $\Lambda(1670)$, which are dynamically generated within $U\chi PT$. At the same time we have done the numerical evaluations and have determined the actual value for these magnitudes. The values obtained are $\mu_{\Lambda(1405)} = +0.2 \sim 0.5\mu_N$, smaller than that of the Λ ($\sim -0.6\mu_N$) and of opposite sign. For the $\Lambda(1670)$ we obtain $\mu_{\Lambda(1670)} \sim -0.29\mu_N$, also smaller than that of the Λ and with the same sign, while for the transition magnetic moment we obtain a value $|\mu_{\Lambda(1670) \to \Lambda(1405)}| \sim 0.023\mu_N$, which leads to a branching ratio of the $\Lambda(1670)$ to $\Lambda(1405)\gamma$ channel of the order of 2×10^{-6}. The results of the $U\chi PT$ method are different from those obtained with the quark models, reflecting the different nature attributed to the resonances in those models. One of the interesting results obtained in this work is the abnormally small decay width for the $\Lambda(1670) \to \Lambda(1405)\gamma$ transition, which differs in two orders of magnitude from the quark model predictions. Short of a measurement of the transition, which could be difficult given the small numbers predicted, even

the determination of an upper bound would provide interesting information about the nature of these resonances.

Acknowledgments

References

[1] N. Isgur and G. Karl, Phys. Rev. D18 (1978) 4187; *ibid.* D20 (1979) 1191; S. Capstick and W. Roberts, Phys. Rev. D49 (1994) 4570.

[2] F. Cano, P. Gonzalez, S. Noguera, B. Desplanques, Nucl. Phys. A603 (1996) 257.

[3] N. Kaiser, P. B. Siegel and W. Weise, Nucl. Phys. A594 (1995) 325.

[4] E. Oset and A. Ramos, Nucl. Phys. A635 (1998) 99.

[5] J.A. Oller and U.G. Meissner, Phys. Lett. B500 (2001) 263.

[6] N. Kaiser, T. Waas and W. Weise, Nucl. Phys. A612 (1997) 297.

[7] J. C. Nacher, A. Parreno, E. Oset, A. Ramos, A. Hosaka and M. Oka, Nucl. Phys. A **678** (2000) 187.

[8] J. Nieves and E. Ruiz Arriola, Phys. Rev. D **64** (2001) 116008.

[9] T. Inoue, E. Oset and M. J. Vicente Vacas, Phys. Rev. C **65** (2002) 035204.

[10] E. Oset, A. Ramos and C. Bennhold, Phys. Lett. B527 (2002) 99-105.

[11] A. Ramos, E. Oset and C. Bennhold, in preparation.

[12] J. A. Oller and E. Oset, Nucl. Phys. A **620** (1997) 438 [Erratum-ibid. A **652** (1997) 407].

[13] D. Cabrera, E. Oset, M.J. Vicente Vacas, Nucl. Phys. A, in print, nucl-th/0011037.

[14] V. Bernard, N. Kaiser and U. G. Meissner, Int. J. Mod. Phys. E4 (1995) 193.

[15] A. Pich, Rep. Prog. Phys. 58 (1995) 563.

[16] U. G. Meissner and S. Steininger, Nucl. Phys. B **499** (1997) 349.

[17] J. Gasser and H. Leutwyler, Nucl. Phys. B250 (1985) 465.

[18] J. C. Nacher, E. Oset, H. Toki and A. Ramos, Phys. Lett. B **461** (1999) 299.

[19] A.J.G. Hey, P.J. Litchfield and R.J. Cashmore, Nucl. Phys. B95 (1975) 516.

[20] See for example, A. Hosaka and H. Toki, "Quarks, baryons and chiral symmetry", World Scientific (2001).
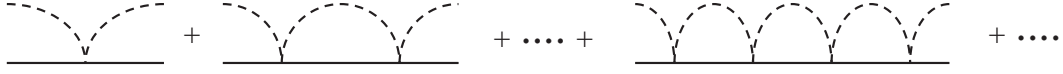
Figure 1: Diagrammatic representation of the Bethe-Salpeter equation in eqs. (1) and (2). Dashed and solid lines denote the meson and the baryon, respectively.
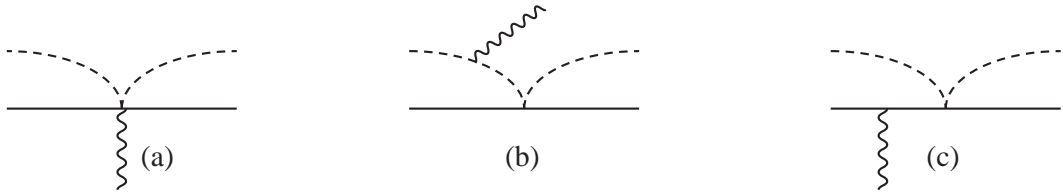
Figure 2: The elementary couplings of the photon to the components of the meson-baryon amplitude. The wavy line denotes the photon.
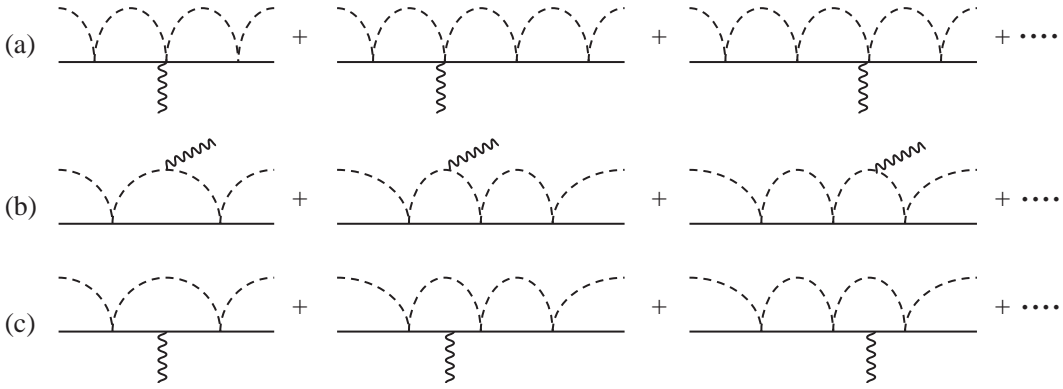
Figure 3: Diagrams for the coupling of the photon to the resonance dynamically generated in meson-baryon scattering.
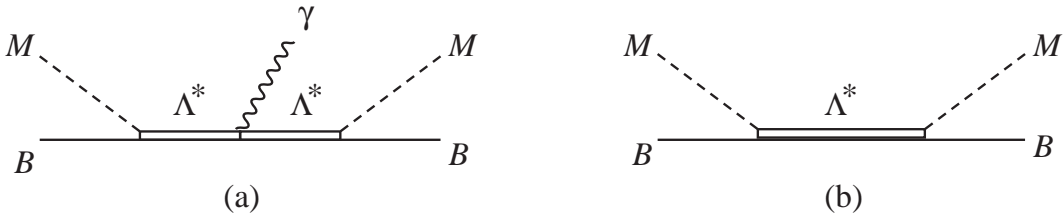

Figure 4: a) Diagrammatic representation of the photon coupling to an explicit resonance. b) Diagrammatic representation of meson-baryon scattering through the explicit resonance.

15
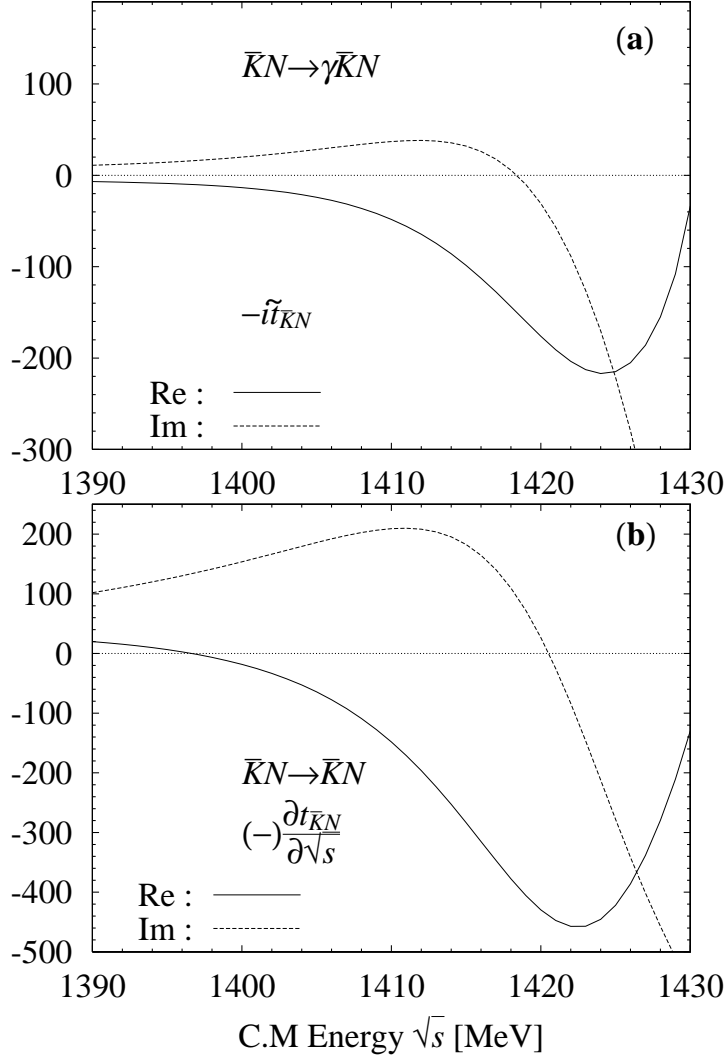
Figure 5: Real and imaginary parts of a) the numerator $-i\tilde{t}_{\bar{K}N}$ in eq.(24) and b) the denominator $-\partial t_{\bar{K}N}/\partial\sqrt{s}$ in eq.(24) around the $\Lambda(1405)$ resonance region in units of m_π^{-2}.
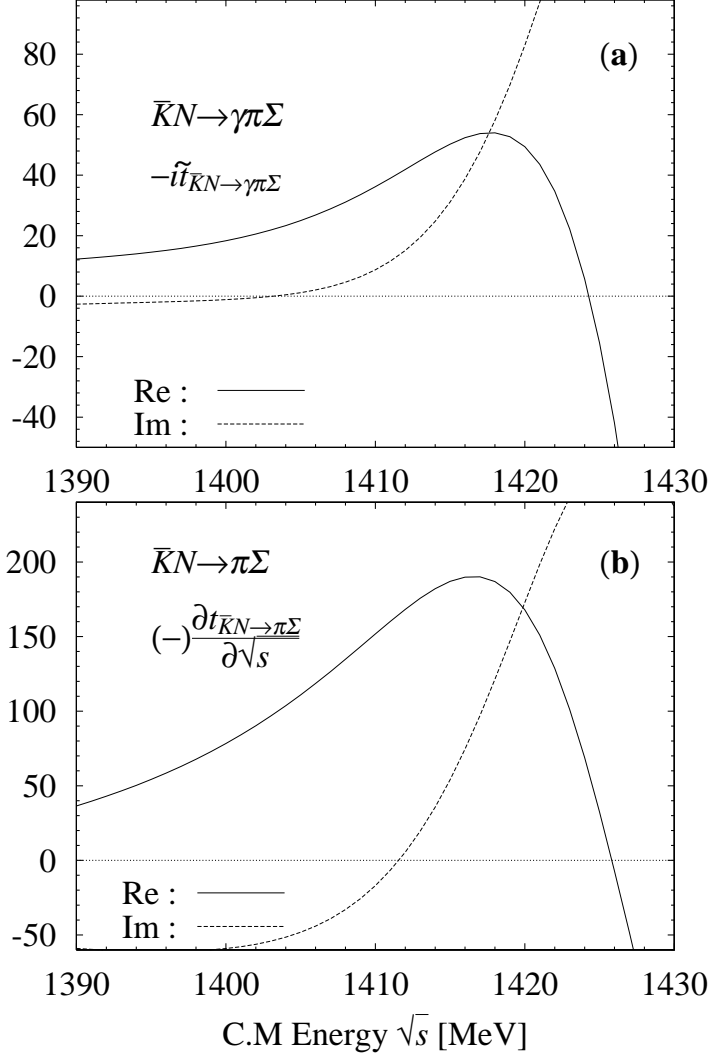
Figure 6: Real and imaginary parts of a) the numerator $-i\tilde{t}_{\bar{K}N\to\gamma\pi\Sigma}$ in eq.(24) and b) the denominator $-\partial t_{\bar{K}N\to\pi\Sigma}/\partial\sqrt{s}$ in eq.(24) around the $\Lambda(1405)$ resonance region in units of m_π^{-2}.
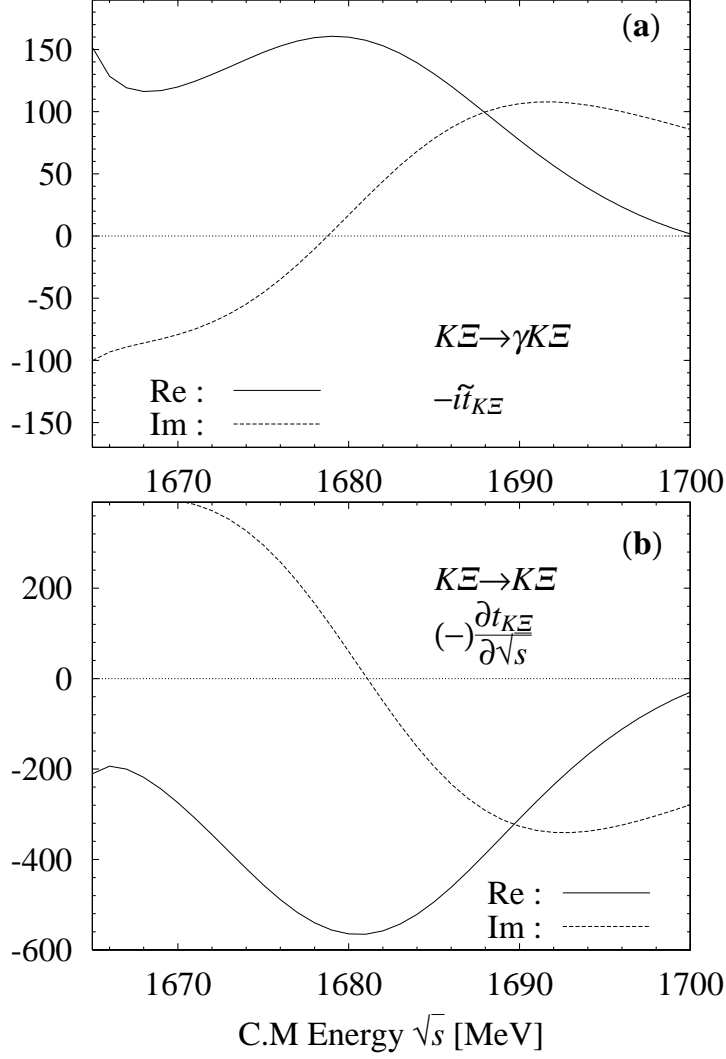
17

Figure 7: Real and imaginary parts of a) the numerator $-i\tilde{t}_{K\Xi}$ in eq.(24) and b) the denominator $-\partial t_{K\Xi}/\partial\sqrt{s}$ in eq.(24) around the $\Lambda(1670)$ resonance region in units of m_π^{-2}.
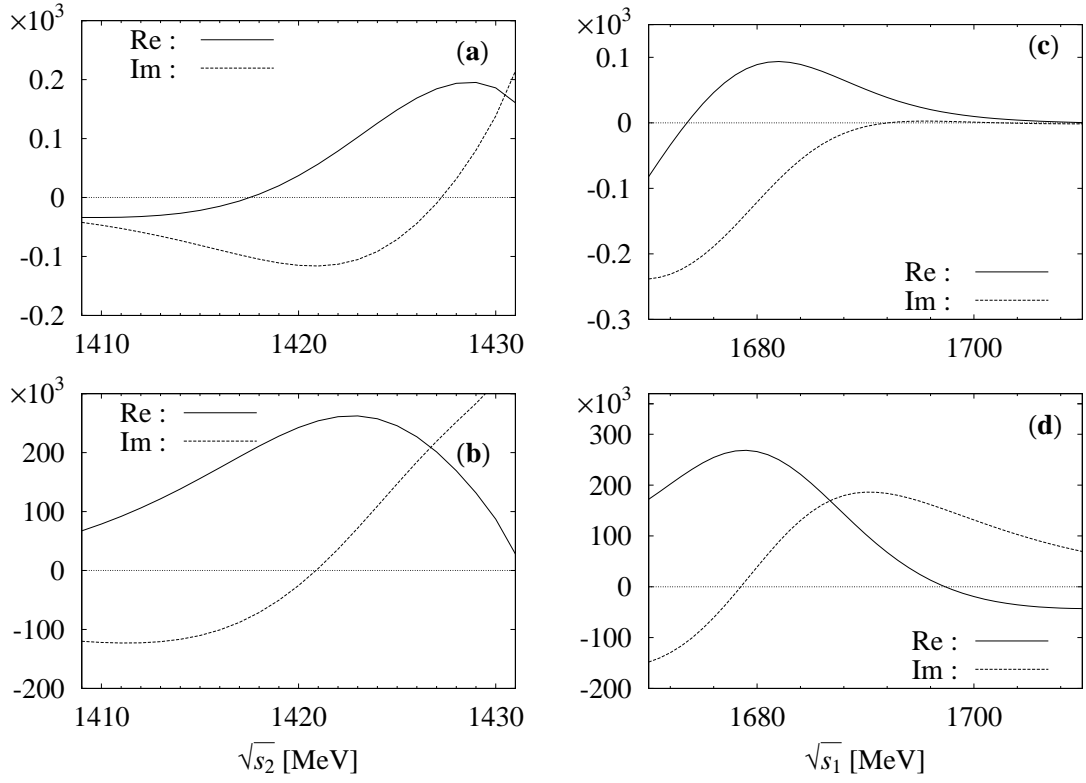
Figure 8: Real and imaginary parts of the numerator, a) and c), and the denominator, b) and d), in eq.(25) in units of m_π^{-4}. In a) and b) $\sqrt{s_1}$ is fixed at 1680 MeV and the numerator and the denominator are functions of $\sqrt{s_2}$. In c) and d) $\sqrt{s_2}$ is fixed at 1420 MeV and the numerator and the denominator are functions of $\sqrt{s_1}$.